8534 J. Med. Chem. 2010, 53, 8534–8545
DOI: 10.1021/jm100941j

Journal of Medicinal Chemistry Article

Discovery of Novel GSK-3β Inhibitors with Potent in Vitro and in Vivo Activities and Excellent Brain Permeability Using Combined Ligand- and Structure-Based Virtual Screening

Mohammad A. Khanfar, Ronald A. Hill, Amal Kaddoumi, and Khalid A. El Sayed*

Department of Basic Pharmaceutical Sciences, College of Pharmacy, University of Louisiana at Monroe, Monroe, Louisiana 71201, United States

Received June 18, 2010

Dysregulation of glycogen synthase kinase (GSK-3β) is implicated in the pathophysiology of many diseases, including type-2 diabetes, stroke, Alzheimer's, and others. A multistage virtual screening strategy designed so as to overcome known caveats arising from the considerable flexibility of GSK-3β yielded, from among compounds in our in-house database and two commercial databases, new GSK-3β inhibitors with novel scaffold structures. The two most potent and selective validated hits, a 2-anilino-5-phenyl-1,3,4-oxadiazole (**24**) and a phenylmethylene hydantoin (**28**), both exhibited nanomolar affinity and selectivity over CDK2 and were potent enough for direct in vivo validation. Both were able to cause significant increases in liver glycogen accumulation in dose-dependent fashion. One also exhibited excellent blood−brain barrier permeability, the other adequate for a lead compound. Analogues of the oxadiazole **24** were synthesized to experimentally corroborate or rule out ligand-bound structures arising from docking studies. SAR results supported one docking study among a number of alternatives.

Introduction

Glycogen synthase kinases 3 (GSK-3α, GSK-3β, and GSK-$3\beta_2$)[a] play vital roles in regulating cell division, stem-cell renewal and differentiation, apoptosis, circadian rhythm, transcription, and insulin action.[1,2] GSK-3β is a 47 kDa nonreceptor serine/threonine kinase, which is a critical modulator of cell fate, neuronal plasticity, and tumorigenesis.[1−3] It was first discovered by virtue of its ability to phosphorylate and inactivate glycogen synthase, the regulatory enzyme of mammalian glycogen synthesis.[3] Its pleiotropic but unique activities have caused GSK-3β to be prosecuted as a theoretically promising pharmacotherapeutic target for the treatment of several human diseases, including type-2 diabetes,[4] CNS disorders including manic depressive disorder and Alzheimer's disease (AD)[5] as well as other neurodegenerative diseases[6] and chronic inflammatory disorders.[7] Lithium was the first GSK-3β inhibitor to be used for therapeutic effect and has been beneficially used in tens of thousands of patients for many years.[1−3] A substantial number of structurally diverse compounds have been reported to inhibit GSK-3β in recent years.[8−17]

One well-known protein substrate of GSK-3β is the microtubule-associated protein, tau. GSK-3β normally phosphorylates tau at specific sites, namely serine 199 and serine 396 (human numbering sequence).[18] GSK-3β seems to be a key mediator in the pathophysiology of AD, in that abnormal hyperphosphorylation of tau (not direct aggregation into filaments under normal cellular status) is now considered to be requisite to neurofibrillary tangle formation, and compromised microtubule stability.[19,20] Moreover, this action of GSK-3β has been reported to be a key effector, possibly the key effector, of the toxic consequences of excessive accumulation of β-amyloid, a protein that aggregates as extracellular amyloid plaques in the brains of AD patients.[21] Exposure of cortical and hippocampal primary neuronal cultures to β-amyloid-derived oligomers induces activation of GSK-3β, tau hyperphosphorylation, and cell death.[22] Consequently, inhibition of GSK-3β renormalizes, in a dose-dependent manner, tau phosphorylation in cells overexpressing tau protein.[23] Suppression of GSK-3β expression by antisense oligonucleotides, or inhibition of its activity with lithium, averts β-amyloid-induced neurodegeneration of cortical and hippocampal primary cultures.[24,26]

In a previous article, we reported the establishment and validation of a pharmacophore model based on marine-derived GSK-3β inhibitors.[11] This model has the characteristic features required for an ideal pharmacophoric query because it incorporates the important interactions known to be required for GSK-3β inhibitors,[27] works in consistent fashion with published GSK-3β pharmacophore models[28−30] and performed quite adequately on our in-house compound database. This query enabled the development of an efficient protocol, reported herein, for discovering new GSK-3β inhibitor scaffolds based on a combination of ligand-based and structure-based (target-based) design. The latter (SBDD) component had already been shown to be absolutely requisite for surmounting the caveats resulting from the known induced-fit flexibility of GSK-3β.[11,27−30]

Several structure databases (our in-house database and also the NCI and Maybridge databases) were drawn on for identifying novel GSK-3β inhibitor scaffolds. The database compounds were subjected to filtering by an extended Lipinski's

*To whom correspondence should be addressed. Phone: +1 318 342 1725. Fax: +1 318 342 1737. E-mail: elsayed@ulm.edu.

[a] Abbreviation: AD, Alzheimer's disease; BBB, blood−brain barrier; CDK2, cyclin-dependent kinase 2; EDCI, *N*-(3-dimethylaminopropyl)-*N*-ethylcarbodiimide; GSK-3β, glycogen synthase kinase-3β; HBA, hydrogen bond acceptor; HBD, hydrogen bond donor; NCI, National Cancer Institute; SAR, structure−activity relationship; SBDD, structure-based drug design; SD, standard deviation; SEM, standard error of mean; VS, virtual screening;

 Published on Web 11/17/2010

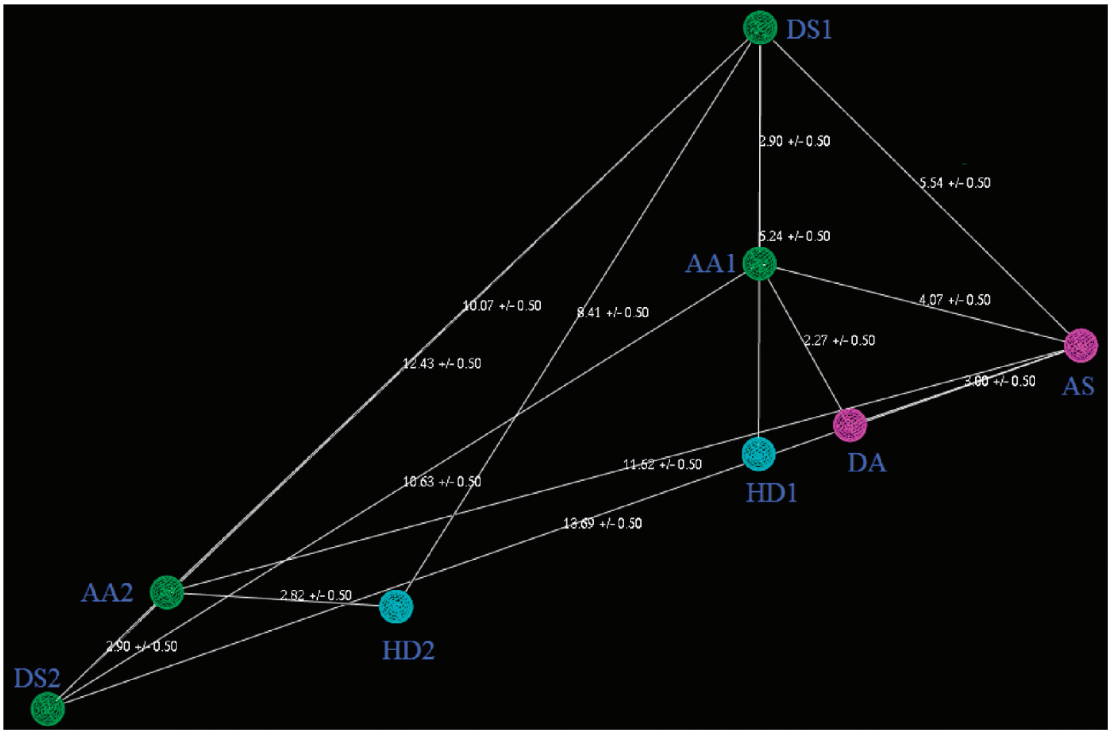

Figure 1. Pharmacophoric features of GSK-3β inhibitors generated by the DISCOtech module and used in the 3D pharmacophoric search. AA-hydrogen bond acceptor atom, DA-hydrogen bond donor atom, HD-hydrophobic center, DS-hydrogen bond donor site, AS-hydrogen bond acceptor site.

rule of five. Pharmacophore-based searching was subsequently carried out, from which initial hits were identified. Docking studies were then undertaken, beginning from multiple disparate X-ray crystallographic structures, with highly restrictive acceptance criteria.[31] Finally, many of the resulting hits were acquired and tested in vitro as inhibitors of recombinant human GSK-3β. Two compounds that exhibited both high potency, and selectivity toward GSK-3β over CDK2 were further evaluated for their in vivo (mice) abilities to enhance hepatic glycogen reserves and to cross the blood−brain barrier (BBB). A 2-anilino-5-phenyl-1,3,4-oxadiazole analogue showed high in vitro and in vivo activities and excellent BBB permeability. To aid in corroborating or else disallowing alternative in silico structures, and for selecting the best hypothesis-generating models for moving forward in lead optimization, 33 new analogues were synthesized using the recently reported, highly efficient one-pot synthesis of substituted 2-amino-1,3,4-oxadiazoles.[32] Structural modifications were mainly focused on the *para* position of the phenyl rings, and substituent selections were based on varying their lipophilic (π) and electronic (σ) characteristics in the manner prescribed by Craig's plot.[33]

Results and Discussion

Virtual Screening. A 3D pharmacophore model built in a previous report was applied in the ligand-based virtual screening.[11] Mapping of this model was based on three marine-derived phenylmethylene hydantoin GSK-3β inhibitors[11] using the DISCOtech module implemented in SYBYL 8.0. Given a set of molecules that are related by their ability to bind to the same protein receptor, DISCOtech identifies features that could be elements in a pharmacophore, employing clique detection to generate pharmacophore hypotheses from up to 300 conformers per molecule.[34−37] After several optimization and refinement steps, a pharmacophore model was obtained that includes the characteristic features known to be requisite and ideal for ATP-competitive GSK-3β inhibition.[27] Using a distance tolerance of 1 Å, five pharmacophoric features were identified, one H-bond donor (HBD), two H-bond acceptors (HBA), and two hydrophobic sites (Figure 1), consistent with previously reported GSK-3β pharmacophores.[28−30] In application, the model performed satisfactorily on the in-house database of active GSK-3β inhibitors and decoys. This model picked 89 active GSK-3β inhibitors and three decoys from among the 200 molecules (100 decoys).

Virtual screening (VS) has for several decades been a fruitful strategy for lead identification. Its use has increased substantially in recent years, especially with the advent of online databases, enabling the discovery of new hits out of millions of virtual structures. VS offers a means to systematically select a small number of compounds, which can then be tested in lower-throughput assays (in-silico (docking, e.g.) or physically), increasing the likelihood of obtaining compounds with desired activities as compared to the more expensive and time-consuming physical high-throughput screening. For the work herein, we employed ligand-based VS using the validated pharmacophoric map, discussed above, followed by structure-based VS (docking), working from three disparate GSK-3β crystallographic structures. As previously mentioned, this two-stage VS protocol (Figure 2) was designed with the intent of overcoming the limitations of each separate method and so as to surmount the caveats known to arise because of induced-fit flexibility with ligand binding to the ATP-binding pocket of GSK-3β.[38,39]

Virtual structures in the in-house (307), National Cancer Institute (NCI, 234,055), and Maybridge (55,541) databases were screened to identify new GSK-3β inhibitors. Our in-house

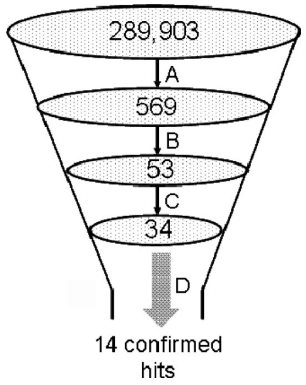

Figure 2. Outline of VS methodology. (A) Compounds downloaded from NCI, Maybridge, and in-house databases were screened using pharmacophore-based VS, filtering also for drug-likeness (see Experimental Section). (B) Molecular docking and ranking by Gold and Surflex-Dock total scores, with selection requiring docking poses that maintained multiple important H-bonding interactions. (C) Available compounds were purchased for testing along with in-house samples. (D) Experimental hit validation was accomplished using a commercial GSK-3β kinase assay kit.

database is composed of compounds of a wide variety of structural classes, mainly of natural products or their semisynthetic or microbial transformation products thereof, which were readily available for testing. Lipinski's Rule of five[31] was opted as the filtration criterion, limiting the range for molecular weight to $\leq$500, calculated octanol−water partition coefficient to $\leq$5, the number of HBDs (OH's and NH's) to $\leq$5, and HBAs (N's and O's) to $\leq$10. Additional filtering restricted the polar surface area to $<$120 Å^2, and the number of rotatable bonds to a maximum of 7. The pharmacophore-based VS combined with these filters resulted in the selection of 314 hits from the NCI database, 194 hits from the Maybridge database, and 61 hits from our in-house database (total 569). This number of compounds remained unwieldy and undoubtedly included a large fraction of false positives; consequently, hits obtained were further screened via molecular docking studies, that is, structure-based investigation, drawing on several inhibitor-bound GSK-3β crystallographic structures, was conducted. Protein induced-fit flexibility with ligand binding and the presence of a conserved water molecule in the active site of GSK-3β render structure-based VS challenging.[38,39] Moreover, the ATP binding site of GSK-3β readily accommodates many structurally diverse ligands in a variety of manners, as evidenced among the multiplicity of cocrystal structures of GSK-3β (including PDB codes 1Q4L, 1Q3W, 1Q5K, 1Q41, 1UV5, 1Q3D, 1PYX, 2OW3) available in the Protein Data Bank. Previously, the PDB structures of GSK-3β were classified into three major groups based on the alternative positioning of Gln 185.[39] Therefore, we selected three different GSK-3β X-ray structures (1Q4L,[27] 1Q5K,[40] and 1UV5[41]) representing each conformational group for our docking VS. We made use of Surflex-Dock software,[42] as implemented in SYBYL 8.0,[43] for the docking studies of 569 hits generated from the 3D pharmacophore search and rule-based filters. Surflex-Dock is a fully automatic flexible molecular docking algorithm that combines the scoring function from the Hammerhead docking strategy with a search engine that relies on a surface-based molecular similarity method as a means to rapidly generate viable putative poses for molecular fragments carved from the ligands via impeded automation algorithms.[42] To maximize the enrichment and minimize the number of false-positive hits, strict criteria were applied to select the refined hits for physical evaluation in a GSK-3β kinase assay: (i) a ligand had to maintain H-bonding interactions with at least three out of four important amino acids (Val 135, Asp 133, Arg 141, and Gln 185) detected in diverse ligand-GSK-3β complexes[27] in at least one of the docking studies using the three above-mentioned crystallographic structures; (ii) a ligand was required to exhibit a binding orientation similar to one or more of the reported cocrystallized inhibitors, to wit, so that the primary heterocyclic ring (HD1 feature in the pharmacophore model, Figure 1) bridged via at least two H-bonds to the hinge region (Asp 133, Tyr 134, and Val 135) of GSK-3β; (iii) a ligand was required to have a binding score equal to or higher than the cocrystallized GSK-3β inhibitors (I-5 in 1Q4L,[27] AR-A014418 in 1Q5K,[40] and 6-bromoindirubin-3′-oxime in 1UV5[41]) in each docking study. With respect to this last criterion, the choice of scoring function is crucial. Even though scoring functions remain vastly deficient with respect to accuracy or even rank-ordering success, heuristic considerations and aggregate experience suggest some that are likely to be more appropriate, versus those almost certain to misinform, in a particular case. Here, because polar interactions are dominant within the GSK-3β active site, scores that consider these interactions are expected to give the most meaningful results. Accordingly, poses generated by Surflex-Dock were best ranked by Gold and Surflex-Dock-total scores.[39] Gold score is a GOLD-like function that focuses on H-bonding interactions, and is known to perform well in situations where significant polar interactions occur.[44,45] Complementarily, Surflex-Dock's total score has been shown to perform well when the ligand makes relatively many discrete intermolecular interactions, which fits this case because the various cocrystallized GSK-3β inhibitors exhibit at least four.[42] A total of 53 hits satisfied the aforementioned conditions, 35 from NCI, 14 from Maybridge, and 9 from our in-house databases. Only 25 from the two external databases were available. Therefore, only 34 hits were physically tested for their ability to inhibit GSK-3β activity (Figure 3, Table 1).

GSK-3β Kinase Assay and Molecular Modeling Studies. The 34 refined hits were tested against recombinant GSK-3β using the Invitrogen Z′-LYTE Kinase Assay kit (Table 1).[46] All compounds were first tested at 10 μM, and hits with percentage inhibition $\geq$50% were further tested to obtain IC_{50} values. A reference compound, the marine β-carboline alkaloid manzamine A, gave an IC_{50} value of 8.4 μM, comparable to literature reports.[47] A total of 14 compounds (41%) were confirmed to be active inhibitors, of which eight were found to have IC_{50} values $<$1 μM. This significant success (24% of experimentally evaluated compounds were true actives with IC_{50} values $<$1 μM) proved the validity and strength of our VS protocol for discovering potent GSK-3β inhibitors. Strikingly, even though the initial pharmacophore model was developed based strictly on a few compounds having a hydantoin scaffold, diverse structural skeletons were picked in the pharmacophoric screen, about 10% of these successfully met the strict criteria from the second (docking) stage, and in turn nearly a fourth of these were found to be submicromolar GSK-3β inhibitors. The three most active hits (**4**, **17**, and **24**) are 9*H*-purine, pyrido[2,3-*d*]pyrimidine and 2-anilino-1,3,4-oxadiazole derivatives, respectively. Other diverse scaffolds, namely 2-thioxothiazolidin-4-one (**16** and **19**), 2,3-dihydro-[1,2,4]triazolo[4,3-*a*]pyrimidine (**21**), 3-hydroxypyridin-2(1*H*)-one (**23**), and a 3,4-dihydro-2*H*-1,3-benzoxazine (**30**)

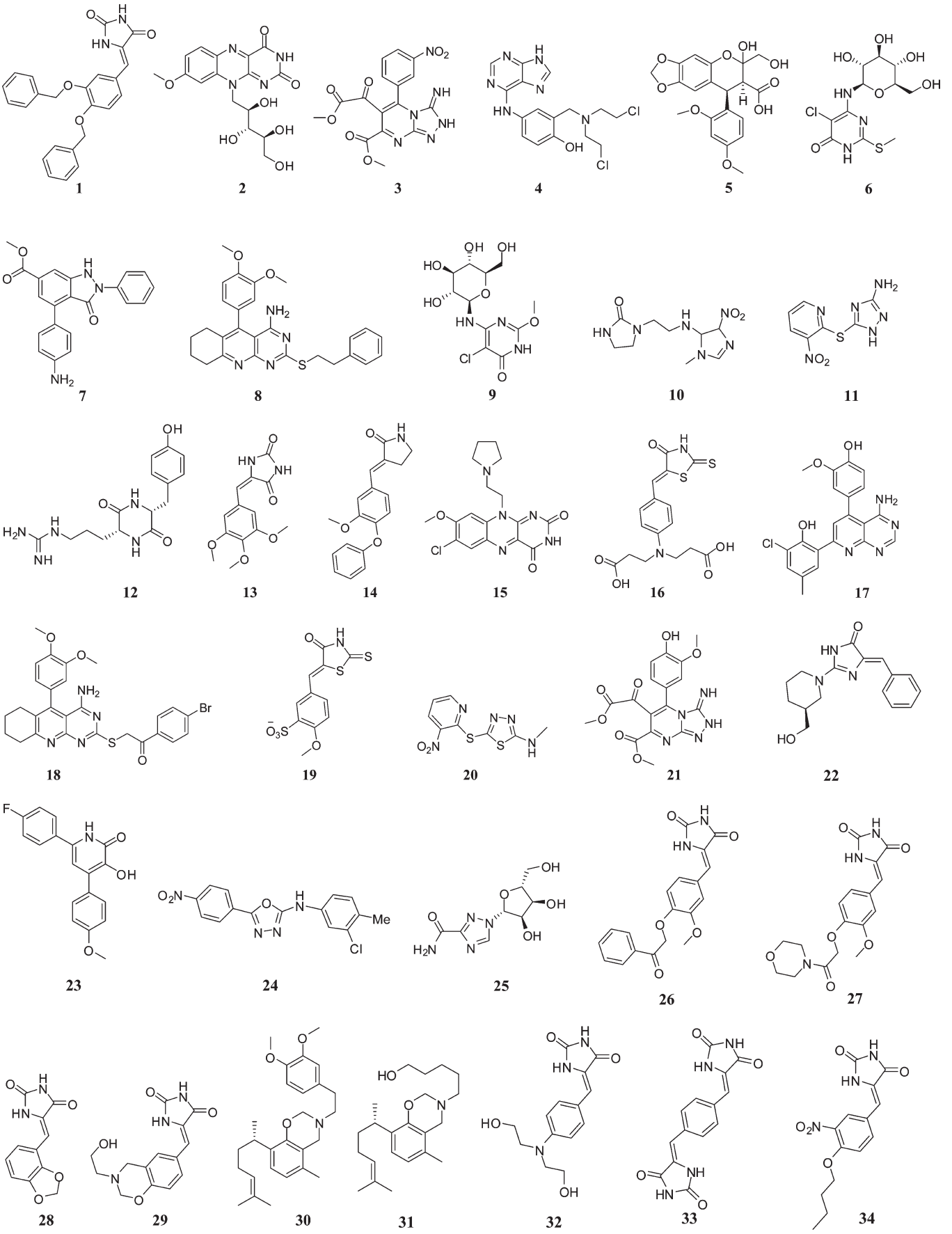

Figure 3. Structures of final hits selected from those identified by the VS scheme.

Table 1. Refined Hits Captured by VS and Their Corresponding in Vitro Kinase Activities

compd	source	% of GSK-3β inhibition at 10 μM	GSK-3β IC_{50} (nM)[a]	% of CDK2 inhibition at 10 μM
1	NCI 146875	71.5	1378 ± 281	ND
2	NCI 330187	33.9	ND	ND
3	NCI 382703	48.5	ND	ND
4	NCI 71283	100	10.8 ± 1.5	98
5	NCI 619690	49.4	ND	ND
6	NCI 609243	71.3	2400 ± 301	ND
7	NCI 382699	34.8	ND	ND
8	NCI 667083	75.0	4700 ± 199	ND
9	NCI 609239	35.2	ND	ND
10	NCI 430239	36.9	ND	ND
11	NCI 1820652	47.6	ND	ND
12	NCI 357032	43.2	ND	ND
13	NCI 122482	81.9	214 ± 17	84
14	NCI 90869	45.4	ND	ND
15	NCI 44685	43.0	ND	ND
16	NCI 690619	90.2	263 ± 77	27
17	NCI 671801	100	113 ± 9	91
18	NCI 667084	35.5	ND	ND
19	NCI 409027	90.4	537 ± 110	ND
20	NCI 1048917	56.2	ND	ND
21	NCI 382704	71.8	2456 ± 491	ND
22	NCI 684340	37.9	ND	ND
23	M S06669SC	96.9	325 ± 13	94
24	M SEW00923SC	100	17 ± 2	22
25	M SEW00923SC	33.3	ND	ND
26	IH	37.6	ND	ND
27	IH	75.5	1975 ± 243	ND
28	IH	94.4	138 ± 26	27
29	IH	45.5	ND	ND
30	IH	91.4	1270 ± 99	ND
31	IH	33.1	ND	ND
32	IH	42.2	ND	ND
33	IH	89.9	2810 ± 113	ND
34	IH	38.6	ND	ND
Manzamine[b]		76.8	8400 ± 739	ND

[a] IC_{50} values for GSK-3β shown are the mean ± SD of duplicate or triplicate measurements. [b] Used as positive control. NCI: National Cancer Institute, M: Maybridge, IH: in-house database, ND: not determined.

were identified. All compounds were stereochemically pure single isomers except compound **2**. This hit was virtually screened as downloaded from the NCI database, with stereochemistry as specified in Figure 3. Compound **2** was found to be inactive (Table 1) and was not investigated further.

The chances of the validated hits to act as noncompetitive or allosteric inhibitors, or alternatively, competitively bind within the substrate-binding pocket, would be very remote for the following reasons: (1) the algorithm by which the hits were discovered, in particular considering the highly restrictive nature of the used in silico docking procedures, and (2) the fact that the observed SAR (from experimental testing of hits in an in vitro kinase assay, and subsequently a functional assay (in vivo liver glycogen content) for the most potent compounds) can be well rationalized by the most robust of the docking models, which were constructed based on a diverse set of X-ray crystallographic structures of ATP-competitive inhibitors bound within the ATP binding pocket of GSK-3β.

CDK2 is the most closely related kinase from a homology perspective (overall 33% amino acid identity),[25] and most reported GSK-3β inhibitors also potently inhibit CDK2, notably excepting a number of anilinomaleimides.[7,12,26] Although dual inhibition of GSK-3β and CDK2 is not necessarily linked to possible side effects, CDK2 was selected to represent other related kinases, which should show low binding affinity toward new GSK-3β hits to avoid possible toxicities. CDK2 is essential for G1 progression and S-phase entry of the cell cycle.[48] Inhibition of CDK2 will arrest the cell cycle and cellular proliferation,[48] which will complicate assessment of therapeutic and toxicological effects of GSK-3β inhibition in GSK-3β-related pathologies, including diabetes, inflammation, neurological disorders, and various neoplastic diseases. Therefore, the affinities of all confirmed hits toward CDK2 were assessed. Excluding hits **24** and **28**, all other potent hits (GSK-3β IC_{50} < 1.0 μM) demonstrated strong inhibition of CDK2 at 10 μM. The 2-anilino-1,3,4-oxadiazole **24** showed a high affinity to GSK-3β (IC_{50} = 17.1 nM) but only inhibited CDK2 by 22% at 10 μM. To structurally understand the high affinity for GSK-3β but not CDK2, compound **24** was docked inside the ATP-binding site of GSK-3β using Surflex-Dock implemented in SYBYL 8.0 (Figure 4). Only one pose, obtained from PDB structure 1UV5, could well explain the SAR obtained from the experimental IC_{50} values of its analogues (vide supra). In this pose, the docking results suggest that oxadiazole **24** binds along the hinge region of GSK-3β, making three hydrogen-bonding interactions to main-chain (backbone) atoms of the protein. Furthermore, in this identified pose, the nitro group of the docked inhibitor occupies the inner part of the ATP pocket; the closest distance between a nitro oxygen and the selectivity residue Leu 132 is only 3.12 Å. Importantly, the model indicates that this nitro group occupies the position of a bound water molecule from the starting PDB structure and thereby interacts with lysine of the Asp 200-Lys 85 salt bridge via an apparent H-bond. The docking study positions the electron-deficient benzene ring so as to interact with the Cys 199 thiol via a charge-transfer interaction. Finally, this pose positions the other end group of **24**, the aniline moiety, with its ring rotated out of the plane from the oxadiazole ring, and so as to occupy a hydrophobic pocket established by Ile 62, Leu 188, and the methyl of Thr 138 (Figure 4A,B).

Similarly, a pose obtained starting from PDB structure 1UV5 well accounts for the experimental SAR among the nine tested phenylmethylene hydantoin analogues. In this pose, structure **28** binds through two hydrogen bonds to the hinge region. The dioxolane ring of **28** is predicted to rest in proximity to the selectivity residue Leu 132, with the *meta*-oxygen bridged via two hydrogen bonds, one to Lys 85 and the other to the backbone N−H of Asp 200. The model furthermore predicts the aromatic ring to stack over the thiol group of Cys 199, at 3.93 Å, positioned for an effective charge transfer interaction (Figure 4C,D).

The GSK-3β active site has been extensively characterized, and two "selectivity residues" versus CDK2 have been identified: Leu 132 and Arg 141.[27] Arg 141 forms a salt bridge with Glu 137, therewith defining the boundary and entrance region to the ATP pocket. The equivalent residues involved in the salt bridge are Lys 89 and Glu 85 in CDK2. The Lys 89 side chain points inward to the ATP pocket, interacting with a main-chain atom from a Gly-rich loop. This arrangement would disallow occupancy by the aniline moiety of **24**. The other selectivity residue that differs between both kinases is Leu 132 in GSK-3β vs Phe 80 in CDK2. Likely, the latter residue and its surrounding structure in CDK2 cannot accommodate, sterically or electronically or both, the nitrobenzene moiety of **24**, whereas the docking study suggests that this group fits exquisitely in GSK-3β (see earlier discussion). A structural basis for the experimentally observed

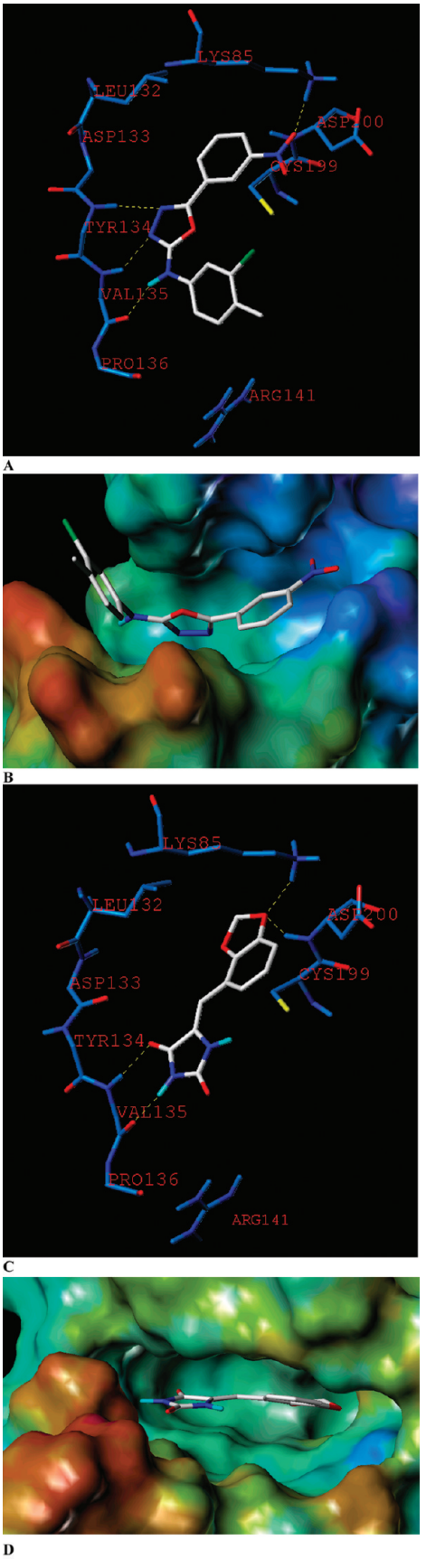

Figure 4. Detailed view of **24** (A/B) and **28** (C/D) docked within the ATP binding site of GSK-3β projected over the Connolly electrostatic potential surface (blue, negative potential; red/brown, positive potential).

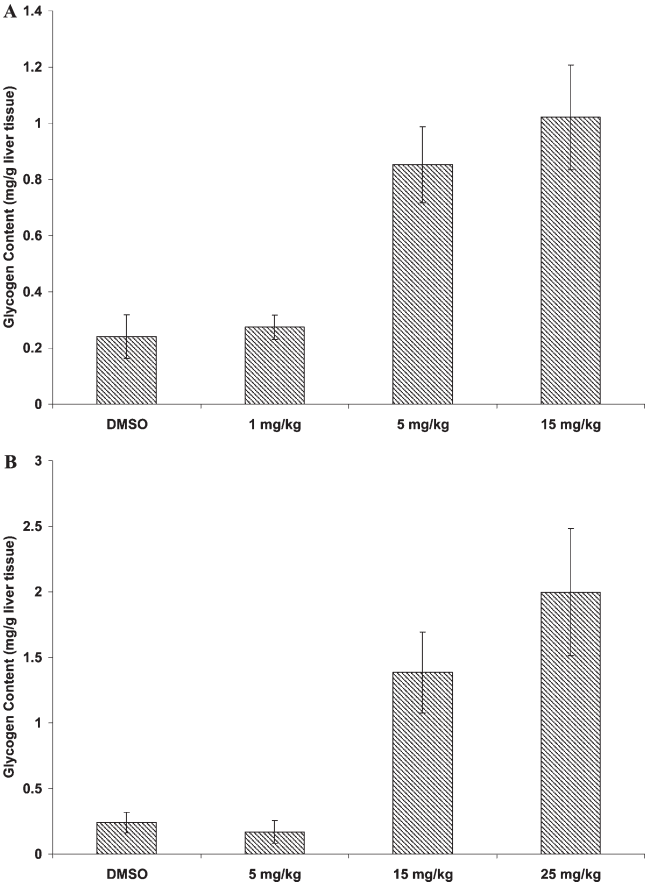

Figure 5. Effect of various doses of **24** (A) and **28** (B) on liver glycogen storage in treated C57BL/6N mice measured 3 h after ip dosing. Error bars indicate SEM, $n = 3$/dose.

high GSK-3β vs CDK2 selectivity of **28** cannot yet be discerned from available structural information.

In Vivo Activities: Hepatic Glycogen Effects and BBB Permeability. GSK-3β plays an important role in controlling hepatic and skeletal muscular glycogen storage in that GSK-3β phosphorylates and inactivates glycogen synthase.[4] Suppression of GSK-3β activity by insulin or small molecule inhibitors increases glycogen storage in muscle and liver.[4,11] A previous study showed that inhibition of GSK-3β selectively reduces the expression of genes for glucose-6-phosphatase and phosphoenolpyruvate carboxykinase.[49] Overall, then, glucose output is reduced and synthesis of glycogen from glucose is increased.[49] These findings indicate that GSK-3β inhibitors may have valuable therapeutic potential for lowering blood glucose levels.

The validated hits **24** and **28**, which exhibited high potency and selectivity for GSK-3β versus CDK2, were tested in mice for their ability to increase liver glycogen reserves. The oxadiazole **24** significantly raised liver glycogen content in a dose-dependent manner ((1, 5, and 15 mg/kg); Figure 5), increasing glycogen content by 3.5- and 4.3-fold at 5 and 15 mg/kg, respectively. Similarly, the phenylmethylene hydantoin **28** increased glycogen reserves at 15 and 25 mg/kg dose levels by 5.8- and 8.3-fold, respectively. Compounds **24** and **28** were well tolerated by the mice; no fatalities were observed.

GSK-3β has also been linked to abnormalities associated with AD, via hyperphosphorylation of the microtubule-associated tau protein. For a GSK-3β inhibitor to counter this abnormality, penetration to CNS neurons is requisite.

Table 2. Plasma and Blood Concentrations of Compounds **24** and **28** at Different Doses[a]

	24			**28**		
	1 mg/kg	5 mg/kg	15 mg/kg	5 mg/kg	15 mg/kg	25 mg/kg
plasma (ng/mL)	14 ± 5	31 ± 12	61 ± 11	< 10	81 ± 8	3734 ± 109
brain (ng/g brain tissue)	38 ± 6	113 ± 54	286 ± 58	< 50	< 50	12113 ± 2182

[a] Data are expressed as mean ± SEM of $n = 3$ using C57BL/6N mice following 3 h of the ip administration.

Scheme 1. Synthesis of 2-Anilino-5-phenyl-1,3,4-oxadiazoles[a]

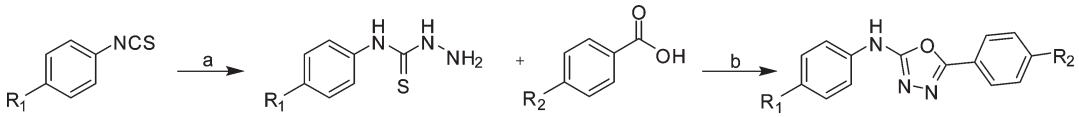

[a] Reagents and conditions: (a) (1) N_2H_4, MeOH, rt, 1 h; (2) 65−80 °C, 20 min; (b) EDCI (3 equiv), CH_2Cl_2, rt, 12 h.

Consequently, we assessed the ability of compounds **24** and **28** to cross the BBB. Using the same mice groups as in the previous experiment, blood samples and brains were collected and drug concentrations measured. Compound **24** was detected in the brain at concentrations higher than in plasma for all three tested doses (1, 5, 15 mg/kg; see Table 2). On the other hand, compound **28** was not detected in plasma or brain samples at 5 mg/kg and was only barely detectable at 15 mg/kg. With the 25 mg/kg dose, however, the plasma levels were substantial, with high penetration into brain. The abrupt, disproportionate increase in plasma concentrations can be rationalized by saturable efflux transport or biotransformation processes or both. Any possible BBB efflux was not yet characterized, as **28** is only a validated hit (albeit a potent one).

Chemistry and SAR of New 2-Anilino-5-phenyl-1,3,4-oxadiazole Derivatives. The validated hit **24** is a 2-anilino-5-phenyl-1,3,4-oxadiazole derivative. Because this compound shows high in vitro and in vivo potency against GSK-3β, outstanding selectivity versus CDK2, and good brain permeability, preliminary SAR studies were merited (i.e., initial hit-to-lead chemistry). Moreover, a main intent was to help assess whether or not any of the well-scoring poses obtained from the docking studies could well explain experimental SAR results and, thus, more profitably offer up further hypotheses for structure-based design efforts in the absence of an X-ray structure.

A variety of synthetic methods for the preparation of 2-amino-1,3,4-oxadiazoles have been reported, almost all involving multistep synthesis. Recently, an efficient one-pot synthesis for preparing substituted 2-amino-1,3,4-oxadiazoles was developed.[32] A carboxylic acid and 4-phenyl-3-thiosemicarbazide are mixed in dichloromethane (DCM) at room temperature with three equivalents of *N*-(3-dimethylaminopropyl)-*N*^{1}-ethylcarbodiimide (EDCI) as coupling reagent, producing the corresponding 2-anilino-5-phenyl-1,3,4-oxadiazoles (Scheme 1). In our hands, as was reported by Chekler et al.,[31] chromatographic purification was not required in most cases. Two of the needed thiosemicarbazides, 4-(4-methoxyphenyl)-3-thiosemicarbazide and 4-(4-nitrophenyl)-3-thiosemicarbazide, were not available commercially but were readily prepared by reacting the corresponding isothiocyanate with hydrazine under reflux in MeOH.

Aromatic substituents were selected so as to systematically vary both lipophilic (π) and electronic (σ) character, as prescribed by Craig's plot.[33] In this study, Cl, CF_3, and NO_2 served as electron-withdrawing ($+\sigma$) and lipophilic ($+\pi$) substituents, CN and SO_2CH_3 as electron-withdrawing and less lipophilic ($+\sigma/-\pi$) ones, OH and OCH_3 as electron-donating and less lipophilic ($-\sigma/-\pi$) substituents, and CH_3 and SCH_3 as electron-donating and more lipophilic ($-\sigma/+\pi$) ones. A total of 33 2-anilino-5-phenyl-1,3,4-oxadiazoles were synthesized and evaluated for their in vitro GSK-3β inhibitory activity (Table 3). For clarity of the following discussion, we denote the aromatic ring derived from the benzoic acids as "ring A" and the one derived from 4-phenyl-3-thiosemicarbazide as "ring B". Substitution of ring A with electron-withdrawing ($+\sigma$) groups increased the activity compared to the unsubstituted ring.

Table 3. Structures and GSK-3β Inhibitory Activities of 2-Anilino-5-phenyl-1,3,4-oxadiazoles

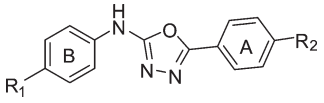

compd	R_1	R_2	IC_{50} (nM) [a]
35	H	H	980 ± 63
36	H	Cl	> 1000
37	H	CF_3	632 ± 29
38	H	CH_3	> 1000
39	H	SCH_3	> 1000
40	H	SO_2CH_3	439 ± 107
41	H	$N(CH_3)_2$	> 1000
42	H	CN	247 ± 55
43	H	NO_2	209 ± 28
44	H	OCH_3	> 1000
45	H	OH	> 1000
46	Cl	H	> 1000
47	Cl	Cl	> 1000
48	Cl	CF_3	> 1000
49	Cl	CH_3	> 1000
50	Cl	SCH_3	855 ± 142
51	Cl	SO_2CH_3	671 ± 89
52	Cl	$N(CH_3)_2$	> 1000
53	Cl	CN	719 ± 17
54	Cl	NO_2	811 ± 58
55	Cl	OCH_3	> 1000
56	Cl	OH	> 1000
57	OCH_3	H	> 1000
58	OCH_3	Cl	534 ± 29
59	OCH_3	CF_3	53 ± 8
60	OCH_3	CH_3	805 ± 192
61	OCH_3	SCH_3	> 1000
62	OCH_3	SO_2CH_3	314 ± 33
63	OCH_3	$N(CH_3)_2$	> 1000
64	OCH_3	CN	18 ± 4
65	OCH_3	NO_2	7 ± 1
66	OCH_3	OCH_3	662 ± 72
67	NO_2	NO_2	710 ± 39

[a] IC_{50} values for GSK-3β shown are the mean ± SD of duplicate or triplicate measurements.

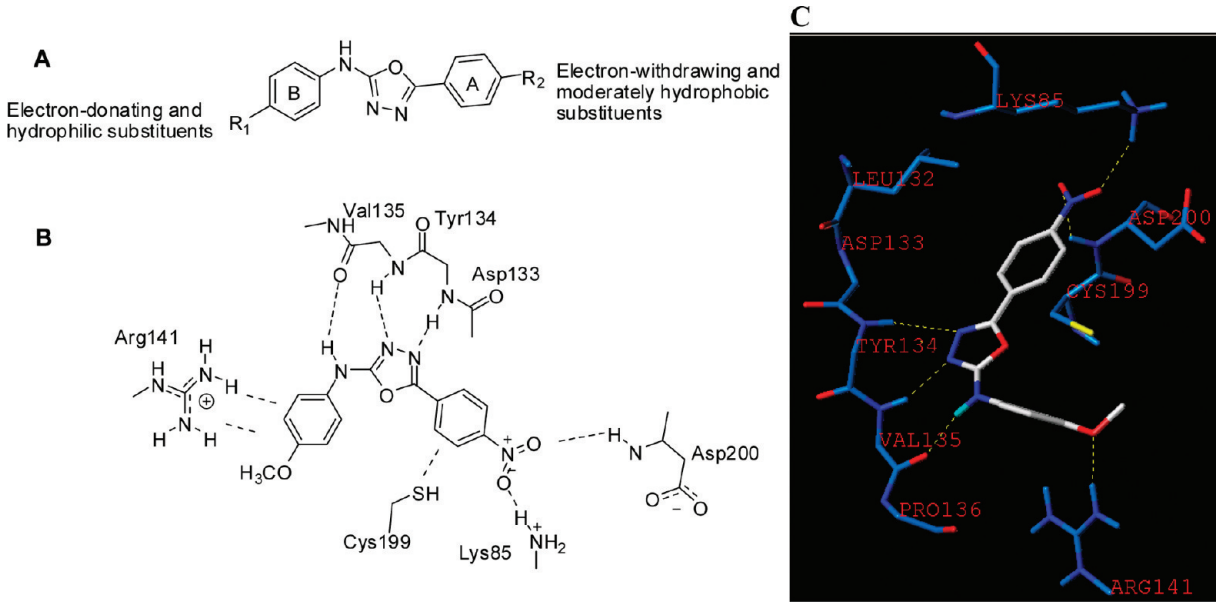

Figure 6. (A) SAR of 2-anilino-5-phenyl-1,3,4-oxadiazole derivatives as defined by Craig's plot substituents. (B) Binding mode of the most active derivative (**65**). (C) Docked pose of **65** in best accord with experimental SAR results.

Compounds **37**, **40**, **42**, and **43**, with CF_3, SO_2CH_3, CN, and NO_2, respectively, on the *para*-position of ring A, were more active than unsubstituted compound **35** or compounds with electron-donating groups (**38** (CH_3), **39** (SCH_3), **41** ($N(CH_3)_2$), or **44** (OCH_3)). Similarly, **51**, **53**, and **54** were more active than **46**, and compounds **58**, **59**, **62**, **64**, and **65** were more active than **57**. On the other hand, CN and NO_2 substitution conferred greater activity than CF_3 and SO_2CH_3: compounds **42** and **43** were more active than **37** and **40**, compounds **53** and **54** were more active than **48**, and compounds **64** and **65** were more active than **59** and **62**. Replacement of NO_2 or CN with Cl dramatically decreased the activity, consistent with docking results suggesting that H-bonding interactions and suitable spatial positioning are of paramount importance. Along with Cl, notably neither SO_2CH_3 nor CF_3 could substitute effectively for CN or NO_2. Methoxy-substitution of ring B was found to generate derivatives having greater activity than those with a halogenated or unsubstituted ring: analogue **64** exhibited 14- and 40-fold greater activity than **42** and **53**, respectively, while **65** was found to be 30- and 116-fold more potent than **43** and **54**, respectively. The two most active compounds, **64** and **65**, with IC_{50} values of 18 and 7 nM, respectively, have *p*-methoxy substitution on ring B. Docking of **65** indicated an H-bond between an N−H of the arginine and a lone pair on the ether oxygen of the methoxy group (Figure 6C). One cannot rule out a secondary edge−face charge transfer interaction between the aromatic ring of **65** and the guanidine-moiety of Arg 141 and, of course, the protein structure was held static in the docking studies, whereas in actuality the protein could adjust to optimize the guanidinium:methoxybenzene interaction. The inductive effect of the OCH_3 substituent might enhance a charge-transfer interaction with the guanidine-moiety of Arg 141; however, the docking results suggest the alternative possibility for an HBA interaction with Thr 138, and an X-ray structure would be required to know which, if either, of these possibilities accounts for the experimental observations.

Conclusions

Herein we present a successful example of employing a multistage VS scheme, beginning with robustly designed pharmacophore-based searching in conjunction with suitable druglikeness filters, followed by docking studies employing rigorous criteria to identify novel compounds with potent GSK-3β inhibitory activities. The validity of the pharmacophore map was established by submitting the corresponding query to a test database of active GSK-3β inhibitors and decoys from a multiplicity of molecule classes. Subsequent docking studies proceeding from three disparate GSK-3β crystallographic structures were then carried out, applying highly restrictive criteria so as to refine the initial screening set into a sufficiently smaller subset as to readily allow experimental evaluations in the kinase assay. The result was that from the 289903 molecules in the combined databases, 34 available compounds from among 59 identified in silico hits were selected for biological testing. With only the very modest effort and expense involved in experimentally screening these 34 compounds, we identified eight interesting new validated hits having nanomolar affinity. Importantly, the hits identified in our study had wide structural diversity, and little true structural similarity to any of the other known GSK-3β inhibitors, highlighting an important merit of the virtual screening approach. The most potent compound, **24**, was a 2-anilino-5-phenyl-1,3,4-oxadiazole, which at first take seems to bear some structural semblance to the highly selective and potent 2-{3-[4-(alkylsulfinyl)phenyl]-1-benzofuran-5-yl}-5-methyl-1,3,4-oxadiazole GSK-3β inhibitor recently divulged by the Takeda group.[50,51] Our in silico results suggest, however, that the roles of oxadiazole in the bridging of **24** is very different than for the Takeda compounds, and **24** has better potency and selectivity. Moreover, the fact that analogues of **24** could be synthesized by a one-step reaction, in contrast to the relatively more complex synthetic schemes required to produce Takeda's oxadiazoles,[50,51] facilitated initial exploration of the SAR. Docking studies in conjunction with the experimental results suggest that prodigious interaction of the optimal nitro substituent with the salt-bridged Lys 85 inside the ATP-binding site of GSK-3β, highly likely along with the displacement of a bound water, confers high affinity, and along with other exquisitely suited structural attributes, excellent selectively versus CDK2. The positive outcomes of our

preliminary in vivo evaluations furthermore suggest that this new series could be of value for further lead optimization toward the design of therapeutically relevant GSK-3β inhibitors.

Experimental Section

General Experimental Procedures. IR spectra were recorded on a Varian 800 FT-IR spectrophotometer (Palo Alto, CA). Optical rotation measurements were carried out on a Rudolph Research Analytical Autopol III polarimeter (Hackettstown, NJ). The ^{1}H and ^{13}C NMR spectra were recorded in DMSO-d_6, using TMS as an internal standard, on a JEOL Eclipse NMR spectrometer (Tokyo, Japan) operating at 400 MHz for ^{1}H and 100 MHz for ^{13}C. The HREIMS experiments were conducted on a 6200-TOF LCMS (Agilent, Santa Clara, CA) equipped with a multimode source (mixed source that can ionize the samples alternatively by ESI or APCI). Analytical HPLC analyses were performed on a Shimadzu HPLC system (Columbia, MD) using a 5 μm C18 column (150 mm $\times$ 4.6 mm id; Agilent, Santa Clara, CA) and isocratic elution (CH_3CN:H_2O; 75:25) with UV detection set at 305 and 220 nm to verify the purity of active virtual hits and synthetic compounds. A purity of $>95\%$ has been established for compounds **1**, **4**, **6**, **13**, **16**, **17**, **19**, **21**, **23**, **24**, **27**, **28**, **30**, **33**, and **34**−**67**. Compound **8** achieved 89% purity level. TLC analyses were carried out on precoated Si gel 60 F_{254} 500 μm TLC plates, using MeOH/CH_2Cl_2 (2:8) as a developing solvent.

General Chemical Reaction Procedures. A. Preparation of 4-Phenyl-3-thiosemicarbazide. The appropriate phenylisothiocyanate (30 mmol) was added, dropwise, over a period of 1 h to a stirred solution of hydrazine (30 mmol) in CH_3OH (8 mL) at 65−80 °C. The stirring of the reaction mixture was continued for 20 min more at the same temperature. The solvent was removed by evaporation in vacuo. The precipitate was collected by filtration and washed with petroleum ether. The compound was used without further purification.[52]

B. Preparation of 2-Anilino-5-phenyl-1,3,4-oxadiazole Derivatives. A carboxylic acid (0.33 mmol), a 4-phenyl-3-thiosemicarbazide (0.33 mmol), and EDCI (182 mg, 1.0 mmol) were mixed in CH_2Cl_2 (15 mL), and the reaction mixture was stirred at room temperature. Product precipitate formed after several hours, and after stirring for a total of 12 h, the precipitate was collected by filtration, washed with dichloromethane (20 mL), and dried on a filtering funnel to afford the desired product.[32]

C. Preparation of Phenylmethylene Hydantoins. Hydantoin (1.0 g, 10 mmol) was dissolved in 10 mL of H_2O while heating at 70 °C in an oil bath with continuous stirring (Scheme 1).[41] The pH was adjusted to 7.0 using saturated $NaHCO_3$. After dissolution was complete, the temperature was then raised to 90 °C. Ethanolamine (0.9 mL, 14.9 mmol) was added, and an equimolar quantity of the corresponding aldehyde as a solution in 2−5 mL of EtOH was then added dropwise with continuous stirring. The solution was refluxed for approximately 5−8 h, during which time a yellow or white precipitate formed. The reaction was monitored hourly by TLC, and when complete depletion of the starting aldehyde was apparent, the mixture was cooled, and the precipitate was collected by filtration and washed with EtOH−H_2O (1:5) before recrystallization from EtOH.

(*Z*)-5-(2,3-Methylenedioxyphenyl)imidazolidine-2,4-dione (28). Compound **28** was prepared according to procedure C to afford 1.67 g of white powder (72%). ^{1}H NMR (DMSO-d_6, 400 MHz) δ 6.12 (s, 2H), 6.31(s, 1H), 6.87 (dd, 1H, J = 1.5, 7.7), 6.90 (dd, 1H, J = 8.0, 7.7), 8.12 (dd, 1H, J = 8.0, 1.5) 10.22 (s, 1H), 11.30 (s, 1H). ^{13}C NMR (DMSO-d_6, 100 MHz) δ 99.8 (CH_2), 114.7 (CH), 116.2 (qC), 120.8 (CH), 121.9 (CH), 122.4 (CH), 124.7 (qC), 147.2 (qC), 147.1 (qC), 158.7 (qC), 162.5 (qC). HREIMS m/z 255.0380 $[M+Na]^+$ (calcd for $C_{11}H_8N_2O_4Na$, 255.0382).

5-(4-(Trifluoromethyl)phenyl)-*N*-phenyl-1,3,4-oxadiazol-2-amine (37). Compound **37** was prepared according to procedure B to afford 8.9 mg of white powder (10%). ^{1}H NMR (DMSO-d_6, 400 MHz) δ 7.04 (dd, 1H, J = 7.3, 1.1), 7.39 (dd, 2H, J = 7.7, 7.3), 7.62 (dd, 2H, J = 7.7, 1.1), 7.96 (d, 2H, J = 8.0), 8.10 (d, 1H, J = 8.0) 10.81 (s, 1H). ^{13}C NMR (DMSO-d_6, 100 MHz) δ 117.8 (CH), 122.7 (qC), 124.3 (CH), 126.8 (CH), 127.9 (CH), 129.4 (CH), 131.2 (qC), 138.1 (qC), 160.7 (qC), 161.5 (qC). HREIMS m/z 306.0830 $[M+H]^+$ (calcd for $C_{15}H_{11}F_3N_3O$, 306.0854).

5-(4-(Methylmercapto)phenyl)-*N*-phenyl-1,3,4-oxadiazol-2-amine (39). Compound **39** was prepared according to procedure B to afford 48 mg of white powder (51%). ^{1}H NMR (DMSO-d_6, 400 MHz) δ 2.50 (s, 1H), 7.02 (d, 1H, J = 7.3), 7.39 (dd, 2H, J = 8.4, 7.3), 7.43 (d, 2H, J = 8.4), 7.63 (d, 2H, J = 8.0), 7.81 (d, 1H, J = 8.0) 10.68 (s, 1H). ^{13}C NMR (DMSO-d_6, 100 MHz) δ 14.7 (CH_3), 117.6 (CH), 120.75 (qC), 122.4 (CH), 126.5 (CH), 129.7 (CH), 139.2 (qC), 142.9 (qC), 158.1 (qC), 160.2 (qC). HREIMS m/z 284.0838 $[M+H]^+$ (calcd for $C_{15}H_{14}N_3OS$, 284.0858).

5-(4-(Methylsulfonyl)phenyl)-*N*-phenyl-1,3,4-oxadiazol-2-amine (40). Compound **40** was prepared according to procedure B to afford 32 mg of white powder (31%). ^{1}H NMR (DMSO-d_6, 400 MHz) δ 3.37 (s, 3H), 7.02 (d, 1H, J = 7.4), 7.37 (dd, 2H, J = 8.9, 7.4), 7.62 (d, 2H, J = 8.9), 8.12 (s, 4H). ^{13}C NMR (DMSO-d_6, 100 MHz) δ 40.1 (CH_3), 117.0 (CH), 122.7 (CH), 129.6 (CH), 130.5 (qC), 139.1 (qC), 140.2 (qC), 159.6 (qC), 160.2 (qC). HREIMS m/z 316.0755 $[M+H]^+$ (calcd for $C_{15}H_{14}N_3O_3S$ 316.0756).

***N*,5-Bis(4-chlorophenyl)-1,3,4-oxadiazol-2-amine (47).** Compound **47** was prepared according to procedure B to afford 42 mg of white powder (42%). ^{1}H NMR (DMSO-d_6, 400 MHz) δ 7.43 (d, 2H, J = 7.0), 7.64 (d, 2H, J = 7.3), 7.66 (d, 2H, J = 7.3), 7.81 (d, 1H, J = 7.0), 7.89 (d, 2H, J = 7.0), 10.92 (s, 1H). ^{13}C NMR (DMSO-d_6, 100 MHz) 122.6 (CH), 124.7 (qC), 127.4 (qC), 128.5 (CH), 129.6 (CH), 129.9 (CH) 134.2 (qC), 137.9 (qC), 159.6 (qC), 161.2 (qC). HREIMS m/z 306.0182 $[M+H]^+$ (calcd for $C_{14}H_{10}Cl_2N_3O$, 306.0201).

***N*-(4-Chlorophenyl)-5-(4-(trifluoromethyl)phenyl)-1,3,4-oxadiazol-2-amine (48).** Compound **48** was prepared according to procedure B to afford 32 mg of white powder (29%). ^{1}H NMR (DMSO-d_6, 400 MHz) δ 7.45 (d, 2H, J = 8.8), 7.65 (d, 2H, J = 8.8), 7.96 (d, 2H, J = 8.4), 8.1 (d, 2H, J = 8.4), 11.02 (s, 1H). ^{13}C NMR (DMSO-d_6, 100 MHz) 120.6 (CH), 124.3 (qC), 124.7 (qC), 125.3 (CH), 127.6 (qC), 128.0 (CH) 129.0 (CH), 135.2 (qC), 143.6 (qC), 160.0 (qC), 161.4 (qC). HREIMS m/z 340.0450 $[M+H]^+$ (calcd for $C_{15}H_{10}ClF_3N_3O$, 340.0464).

***N*-(4-Chlorophenyl)-5-*p*-tolyl-1,3,4-oxadiazol-2-amine (49).** Compound **49** was prepared according to procedure B to afford 26 mg of white powder (28%). ^{1}H NMR (DMSO-d_6, 400 MHz) δ 2.39 (s, 3H), 7.39 (d, 2H, J = 8.1), 7.43 (d, 2H, J = 8.1), 7.63 (d, 2H, J = 8.4), 7.79 (d, 2H, J = 8.4), 10.86 (s, 1H). ^{13}C NMR (DMSO-d_6, 100 MHz) 22.1 (CH_3), 120.1 (CH), 124.2 (qC), 128.7 (CH), 129.3 (CH), 129.9 (CH), 131.0 (qC) 135.1 (qC), 135.4 (qC), 161.6 (qC), 162.0 (qC). HREIMS m/z 286.0731 $[M+H]^+$ (calcd for $C_{15}H_{13}ClN_3O$, 286.0747).

***N*-(4-Chlorophenyl)-5-(4-(methylmercapto)phenyl)-1,3,4-oxadiazol-2-amine (50).** Compound **50** was prepared according to procedure B to afford 36 mg of white powder (34%). ^{1}H NMR (DMSO-d_6, 400 MHz) δ 2.55 (s, 3H), 7.42 (d, 2H, J = 8.7), 7.45 (d, 2H, J = 8.8), 7.64 (d, 2H, J = 8.8), 7.81 (d, 2H, J = 8.7), 11.04 (s, 1H). ^{13}C NMR (DMSO-d_6, 100 MHz) 14.6 (CH_3), 114.2 (CH), 124.5 (qC), 128.1 (CH), 129.2 (CH), 129.7 (CH), 131.2 (qC) 134.4 (qC), 143.5 (qC), 160.6 (qC), 161.8 (qC). HREIMS m/z 318.0451 $[M+H]^+$ (calcd for $C_{15}H_{13}ClN_3OS$, 318.0468).

***N*-(4-Chlorophenyl)-5-(4-(methylsulfonyl)phenyl)-1,3,4-oxadiazol-2-amine (51).** Compound **51** was prepared according to procedure B to afford 41 mg of white powder (36%). ^{1}H NMR (DMSO-d_6, 400 MHz) δ 7.45 (d, 2H, J = 8.8), 7.65 (d, 2H, J = 8.8), 8.13 (s, 4H), 11.04 (s, 1H). ^{13}C NMR (DMSO-d_6, 100 MHz) 43.1 (CH_3), 114.2 (CH), 124.5 (qC), 128.1 (CH), 129.2 (CH), 129.7 (CH), 131.2 (qC) 134.4 (qC), 143.5 (qC), 160.6 (qC), 161.8 (qC). HREIMS m/z 350.0369 $[M+H]^+$ (calcd for $C_{15}H_{13}ClN_3O_3S$, 350.0366).

***N*-(4-Chlorophenyl)-5-(4-(dimethylamino)phenyl)-1,3,4-oxadiazol-2-amine (52).** Compound **52** was prepared according to

procedure B to afford 19 mg of white powder (19%). ^{1}H NMR (DMSO-d_6, 400 MHz) δ 3.01 (s, 6H), 6.83 (d, 2H, J = 8.8), 7.40 (d, 2H, J = 8.8), 7.62 (d, 2H, 8.8), 7.69 (d, 2H, 8.8), 10.69 (s, 1H). ^{13}C NMR (DMSO-d_6, 100 MHz) 40.5 (CH_3), 119.4 (CH), 126.3 (qC), 126.9 (CH), 128.7 (CH) 128.7 (qC), 129.6 (CH), 137.9 (qC) 143.0 (qC), 157.5 (qC), 160.7 (qC). HREIMS m/z 315.1016 $[M+H]^+$ (calcd for $C_{16}H_{16}ClN_4O$, 315.1013).

4-(5-(4-Chlorophenyl)-1,3,4-oxadiazol-2-ylamino)benzonitrile (53). Compound **53** was prepared according to procedure B to afford 38 mg of white powder (39%). ^{1}H NMR (DMSO-d_6, 400 MHz) δ 7.44 (d, 2H, J = 8.7), 7.65 (d, 2H, J = 8.7), 8.05 (s, 4H), 11.09 (s, 1H). ^{13}C NMR (DMSO-d_6, 100 MHz) 113.5 (qC), 119.4 (CH), 126.2 (qC), 126.7 (CH) 127.9 (qC), 128.3 (qC), 129.6 (CH) 133.9 (CH), 138.5 (qC), 158.6 (qC), 161.4 (qC). HREIMS m/z 297.0546 $[M+H]^+$ (calcd for $C_{15}H_{10}ClN_4O$, 297.0543).

***N*-(4-Chlorophenyl)-5-(4-nitrophenyl)-1,3,4-oxadiazol-2-amine (54).** Compound **54** was prepared according to procedure B to afford 61 mg of orange powder (61%). ^{1}H NMR (DMSO-d_6, 400 MHz) δ 7.44 (d, 2H, J = 8.8), 7.65 (d, 2H, J = 8.8), 8.13 (d, 2H, J = 8.4), 8.38 (d, 2H, J = 8.3), 11.08 (s, 1H). ^{13}C NMR (DMSO-d_6, 100 MHz) 56.3 (CH_3), 117.2 (CH), 122.5 (CH), 125.3 (qC) 127.9 (CH), 129.2 (CH), 129.4 (qC) 133.5 (qC), 155.5 (qC), 158.5 (qC), 161.4 (qC). HREIMS m/z 317.0430 $[M+H]^+$ (calcd for $C_{14}H_{10}ClN_4O_3$, 317.0441).

5-(4-Chlorophenyl)-*N*-(4-methoxyphenyl)-1,3,4-oxadiazol-2-amine (58). Compound **58** was prepared according to procedure B to afford 80 mg of white powder (80%). ^{1}H NMR (DMSO-d_6, 400 MHz) δ 3.74 (s, 3H), 7.53 (d, 2H, J = 8.8), 7.64 (d, 2H, J = 9.1), 7.88 (d, 2H, J = 8.8), 7.94 (d, 2H, J = 9.1), 10.49 (s, 1H). ^{13}C NMR (DMSO-d_6, 100 MHz) 55.8 (CH_3), 114.9 (CH), 119.3 (CH), 123.4 (qC), 127.8 (CH), 130.1 (CH), 132.3 (qC), 136.0 (qC), 155.1 (qC), 158.5 (qC), 160.9 (qC). HREIMS m/z 302.0694 $[M+H]^+$ (calcd for $C_{15}H_{13}ClN_3O_2$, 302.0696).

***N*-(4-Methoxyphenyl)-5-(4-(trifluoromethyl)phenyl)-1,3,4-oxadiazol-2-amine (59).** Compound **59** was prepared according to procedure B to afford 69 mg of white powder (63%). ^{1}H NMR (DMSO-d_6, 400 MHz) δ 3.74 (s, 3H), 6.96 (d, 2H, J = 9.2), 7.54 (d, 2H, J = 9.2), 7.95 (d, 2H, J = 8.4), 8.08 (d, 2H, J = 8.4), 10.6 (s, 1H). ^{13}C NMR (DMSO-d_6, 100 MHz) δ 55.8 (CH_3), 114.9 (CH), 119.3 (CH), 123.4 (qC), 125.3 (qC), 126.7 (CH), 126.9 (CH), 129.4 (qC) 132.2 (qC), 155.2 (qC), 157.1 (qC), 161.2 (qC). HREIMS m/z 336.0965 $[M+H]^+$ (calcd for $C_{16}H_{13}F_3N_3O_2$, 336.0960).

***N*-(4-Methoxyphenyl)-5-*p*-tolyl-1,3,4-oxadiazol-2-amine (60).** Compound **60** was prepared according to procedure B to afford 80 mg of white powder (80%). ^{1}H NMR (DMSO-d_6, 400 MHz) δ 2.39 (s, 3H), 3.74 (s, 3H), 7.33 (d, 2H, J = 8.6), 7.64 (d, 2H, J = 9.1), 7.92 (d, 2H, J = 9.1), 7.93 (d, 2H, J = 8.6), 10.39 (s, 1H). ^{13}C NMR (DMSO-d_6, 100 MHz) 55.8 (CH_3), 114.9 (CH), 119.3 (CH), 123.4 (qC), 127.8 (CH), 130.1 (CH), 132.3 (qC), 136.0 (qC), 155.1 (qC), 158.5 (qC), 160.9 (qC). HREIMS m/z 282.1230 $[M+H]^+$ (calcd for $C_{16}H_{16}N_3O_2$, 282.1243).

***N*-(4-Methoxyphenyl)-5-(4-(methylthio)phenyl)-1,3,4-oxadiazol-2-amine (61).** Compound **61** was prepared according to procedure B to afford 54 mg of white powder (54%). ^{1}H NMR (DMSO-d_6, 400 MHz) δ 2.54 (s, 3H), 3.73 (s, 3H), 6.94 (d, 2H, J = 9.2), 7.43 (d, 2H, J = 8.7), 7.52 (d, 2H, J = 9.1), 7.79 (d, 2H, J = 8.7), 10.43 (s, 1H). ^{13}C NMR (DMSO-d_6, 100 MHz) 14.7 (CH_3), 55.8 (CH_3), 114.8 (CH), 116.5 (CH), 127.8 (CH), 129.4 (qC), 129.7 (CH), 132.5 (qC), 136.3 (qC), 155.4 (qC), 158.5 (qC), 161.2 (qC). HREIMS m/z 314.0964 $[M+H]^+$ (calcd for $C_{16}H_{16}N_3O_2S$, 314.0963).

***N*-(4-Methoxyphenyl)-5-(4-(methylsulfonyl)phenyl)-1,3,4-oxadiazol-2-amine (62).** Compound **62** was prepared according to procedure B to afford 68 mg of white powder (60%). ^{1}H NMR (DMSO-d_6, 400 MHz) δ 3.26 (s, 3H), 3.71 (s, 3H), 6.93 (d, 2H, J = 8.8), 7.50 (d, 2H, J = 8.8), 8.08 (s, 4H), 10.59 (s, 1H). ^{13}C NMR (DMSO-d_6, 100 MHz) 43.8 (CH_3), 55.8 (CH_3), 114.9 (CH), 119.4 (CH), 126.7 (CH), 128.8 (CH), 128.9 (qC) 132.2 (qC), 142.70 (qC), 155.2 (qC), 157.1 (qC), 161.2 (qC). HREIMS m/z 346.0862 $[M+H]^+$ (calcd for $C_{16}H_{16}N_3O_4S$, 346.0862).

5-(4-(Dimethylamino)phenyl)-*N*-(4-methoxyphenyl)-1,3,4-oxadiazol-2-amine (63). Compound **63** was prepared according to procedure B to afford 18 mg of white powder (16%). ^{1}H NMR (DMSO-d_6, 400 MHz) δ 2.99 (s, 6H), 3.73 (s, 3H), 6.82 (d, 2H, J = 7.0), 6.94 (d, 2H, J = 7.0), 7.51 (d, 2H, J = 7.0), 7.67 (d, 2H, J = 7.0), 10.27 (s, 1H). ^{13}C NMR (DMSO-d_6, 100 MHz) 40.3 (CH_3), 55.8 (CH_3), 111.6 (qC), 112.5 (CH), 114.9 (CH), 118.9 (CH), 127.3 (CH), 129.4 (qC) 133.2 (qC), 155.6 (qC), 158.9 (qC), 159.2 (qC). HREIMS m/z 311.1519 $[M+H]^+$ (calcd for $C_{17}H_{19}N_4O_2$, 311.1508).

***N*,5-Bis(4-methoxyphenyl)-1,3,4-oxadiazol-2-amine (66).** Compound **66** was prepared according to procedure B to afford 38 mg of white powder (39%). ^{1}H NMR (DMSO-d_6, 400 MHz) δ 3.73 (s, 3H), 3.84 (s, 3H), 6.96 (d, 2H, J = 9.0), 7.13 (d, 2H, J = 8.8), 7.52 (d, 2H, J = 9.0), 7.81 (d, 2H, J = 8.8), 10.40 (s, 1H). ^{13}C NMR (DMSO-d_6, 100 MHz) 55.8 (CH_3), 65.0 (CH_3), 114.9 (CH), 115.4 (CH), 117.0 (qC), 119.0 (CH), 127.8 (CH), 133.6 (qC), 154.9 (qC), 158.0 (qC), 160.3 (qC), 161.8 (qC). HREIMS m/z 298.1181 $[M+H]^+$ (calcd for $C_{16}H_{16}N_3O_3$, 298.1192).

Molecular Modeling. Three-dimensional structure building and all modeling were carried out using components within the SYBYL program package, version 8.0,[43] installed on Dell desktop workstation equipped with dual 2.0 GHz Intel Xeon processor running the Red Hat Enterprise Linux (version 5) operating system. Energy minimizations were performed using the Tripos force field with a distance-dependent dielectric and the Powell conjugate gradient algorithm with a convergence criterion of 0.01 kcal/(mol-Å). Partial atomic charges were computed using the semiempirical AM1 approach within the program MOPAC 6.0. Kinase structures were prepared using the Biopolymer-Prepare module within SYBYL 8.0; hydrogen atoms were added, the protonation states of charged residues within the ATP-binding site of GSK-3β were inspected, and if necessary, altered as appropriate, and AMBER7 FF99 charges were loaded onto kinase structures. In preliminary trials, docking studies gave better results (docking scores and optimum binding orientation and interactions) in the absence of all but one of the water molecules; therefore, structure-based virtual screening was conducted without water molecules, except the conserved water molecule (H2104).

Virtual Screening and Molecular Docking. As outlined in Figure 2, NCI (number of molecules: 234055), Maybridge (55541), and in-house databases (307) were searched for new hits by employing the developed pharmacophoric queries, as described in a previous report.[11] Prior filtering was carried out applying Lipinski's rule of five[31] and also restricting the number of rotatable bonds to a maximum of 7 and the polar surface area to $\leq$120 Å^2. A number of hits were obtained from each of the databases, and these were further screened using molecular docking studies with Surflex-Dock version 2.0, interfaced with SYBYL 8.0, docking the compounds to the ATP binding site of GSK-3β. The 3D kinase structures were taken from the Brookhaven Protein Databank (PDB code: 1Q4L, 1Q5K, 1UV5). Surflex-Dock employs an idealized active site ligand (protomol) as a target to generate putative poses of molecules or molecular fragments. These putative poses were scored using the Hammerhead and Gold score scoring functions.

In Vitro GSK-3β and CDK2 Inhibitory Activity Assay Using Z′-LYTE Kinase Assay Kit.[46] Recombinant GSK-3β and CDK2 were purchased from Invitrogen (Carlsbad, CA). The GSK-3β and CDK2 kinase assays were carried out with the Invitrogen Z′-LYTE Kinase Assay kit. The assay was optimized for use with GSK-3β as described in the Invitrogen protocol. The GSK-3β concentration was optimized to obtain the desired percent phosphorylation with an acceptable Z'-factor value, which indicates the quality of an assay; Z'-factor values of 0.5 or greater classify an assay as excellent. A Z'-factor value of 0.74 was obtained at final kinase and ATP concentrations of 50 ng/mL and 15 μM, respectively. Tested concentrations ranged from 1 nM to 10 μM distributed log-linearly across the concentration range, and at least two data points from each

concentration were collected. The IC_{50} value for each experiment was obtained using nonlinear regression of the log(concentration) versus percent inhibition values (GraphPad Prism 5.0). Assays were conducted in triplicate, average values were calculated, and no outliers were removed.

In-Vivo Evaluation. Six-week-old male C57BL/6N mice with weights averaging 22 g were assigned into seven groups in randomized fashion, and fed ad libitum with standard food and water, except when fasting was included in the course of a study. All animals were housed under the same conditions. On the day of the experiment, food and water were removed 4 h before the injection. Three groups (3 mice/group) were used to investigate each of the two test compounds (**24** and **28**), with an additional group ($n = 3$) serving as control. Animals were injected intraperitoneally (ip) with one of three doses (1, 5, and 15 mg/kg for compound **24**; 5, 15, and 25 mg/kg for compound **28**). The control group was injected ip with the PBS vehicle ($n = 3$). After 3 h, blood, liver, and brain were rapidly collected.

Determination of Liver Glycogen. Liver glycogen content was characterized following a reported procedure.[53] Briefly, livers were removed immediately after the animals were killed and were homogenized (IKA-T8 Ultra-Turrax, Germany) in an appropriate volume of 5% trichloroacetic acid (TFA) for 5 min. The homogenate was centrifuged (Eppendorf centrifuge 5804 R, Germany) at 3000 rpm for 5 min. The supernatant fluid was filtered using acid-washed paper, and the residues were homogenized again with another volume of 5% TFA for 1−3 min to ensure relatively complete extraction of glycogen. The glycogen contained in 1.0 mL of this filtrate was precipitated using ethanol (95%, 5 mL), incubating in a water bath at 37−40 °C for 3 h. Upon centrifugation at 3000 rpm for 15 min, the clear liquid was gently decanted from the packed glycogen, and the tubes were allowed to drain in an inverted position for 10 min. The glycogen was redissolved in distilled water (2 mL), and the solution mixed with 10 mL of anthrone reagent (0.05% anthrone, 1.0% thiourea in 72% H_2SO_4). The mixture was incubated in boiling water for 30 min, and subsequently, the absorbance was measured spectrophotometrically at 620 nm (Cintra 20, GBC). Blank and standard solutions were prepared, respectively, by adding 10 mL of anthrone reagent to 2 mL of H_2O (blank) or to 2 mL of glucose solution (standard) containing 0.1 mg of glucose in saturated benzoic acid. The liver glycogen content was estimated using the following formula:

$$\text{amount (mg) of glycogen in liver tissue} = (\text{DU/DS}) \times (\text{volume of extract (mL)/weight of liver tissue (g)}) \times 0.09$$

where DU is the absorbance of the unknown sample and DS is the absorbance of the glucose standard.

Brain and Plasma Concentration in Mice. Compounds **24** and **28** were administered to fasted C57BL/6N mice as described above. About 3 h after ip injection, blood and brain samples were collected. The blood samples were centrifuged to obtain the plasma fraction. Brain samples were homogenized in saline to obtain the brain homogenate. The plasma and brain homogenate samples were deproteinized with an equal volume of CH_3CN. Compound concentrations in the supernatant were measured using a Shimadzu HPLC system (Columbia, MD) consisting of a SIL 20-A_{HT} autosampler, SPD-20A UV/vis detector, and LC-20AB pump connected to a Dgu-20A_3 degasser. Data acquisition was achieved by LC Solution software version 1.22 SP1. Separations were achieved on an Agilent 5-μm C18 column (150 mm × 4.6 mm id). Chromatographic conditions for compound **24**: mobile phase of CH_3CN-H_2O (75:25) delivered at 1.0 mL/min, detection wavelength 305 nm. Chromatographic conditions for **28**: CH_3CN-H_2O (40:60) delivered at 1.0 mL/min, detection at 318 nm.

Acknowledgment. This study was supported in part by the Louisiana Biomedical Research Network.

Supporting Information Available: Analytical data of compounds **1**, **4**, **6**, **8**, **13**, **16**, **17**, **19**, **21**, **23**, **24**, **27**, **28**, **30**, and GSK-3β inhibitory activity graphs of **24** and **28**. This material is available free of charge via the Internet at http://pubs.acs.org.

References

(1) Ishiguro, K.; Shiratsuchi, A.; Sato, S.; Omori, A.; Arioka, M.; Kobayashi, S.; Uchida, T.; Imahori, K. Glycogen synthase kinase 3 beta is identical to tau protein kinase I generating several epitopes of paired helical filaments. *FEBS Lett*. **1993**, *325*, 167–172.

(2) (a) Lovestone, S.; Reynolds, C. H.; Latimer, D.; Davis, D. R.; Anderton, B. H.; Gallo, J.-M.; Hanger, D.; Mulot, S.; Marquardt, B. Alzheimer's disease-like phosphorylation of the microtubule-associated protein tau by glycogen synthase kinase-3 in transfected mammalian cells. *Curr. Biol*. **1994**, *4*, 1077–1086. (b) Klein, P. S.; Melton, D. A. A molecular mechanism for the effect of lithium on development. *Proc. Natl. Acad. Sci. U.S.A*. **1996**, *93*, 8455–8459. (c) Pap, M.; Cooper, G. M. Role of glycogen synthase kinase-3 in the phosphatidylinositol 3-kinase/Akt cell survival pathway. *J. Biol. Chem*. **1998**, *273*, 19929–19932.

(3) Welsh, G. I.; Proud, C. G. Glycogen synthase kinase-3 is rapidly inactivated in response to insulin and phosphorylates eukaryotic initiation factor eIF-2B. *Biochem. J*. **1993**, *294*, 625–629.

(4) Wagman, A. S.; Johnson, K. W.; Bussiere, D. E. Discovery and development of GSK3 inhibitors for the treatment of type 2 diabetes. *Curr. Pharm. Des*. **2004**, *10*, 1105–1137.

(5) Li, X.; Lu, F.; Tian, Q.; Yang, Y.; Wang, Q.; Wang, J. Z. Activation of glycogen synthase kinase-3 induces Alzheimer-like tau hyperphosphorylation in rat hippocampus slices in culture. *J. Neural Transm*. **2006**, *113*, 93–102.

(6) Neary, J. T. Kang, Yuan. P2 purinergic receptors signal to glycogen synthase kinase-3beta in astrocytes. *J. Neurosci. Res*. **2006**, *84*, 515–524.

(7) Martinez, A.; Castro, A.; Dorronsoro, I.; Alonso, M. Glycogen synthase kinase 3 (GSK-3) inhibitors as new promising drugs for diabetes, neurodegeneration, cancer, and inflammation. *Med. Res. Rev*. **2002**, *22*, 373–384.

(8) Martinez, A.; Alonso, M.; Castro, A.; Perez, C.; Moreno, F. J. First non-ATP competitive glycogen synthase kinase 3beta (GSK-3beta) inhibitors: thiadiazolidinones (TDZD) as potential drugs for the treatment of Alzheimer's disease. *J. Med. Chem*. **2002**, *45*, 1292–1299.

(9) Naerum, L.; Norskov-Lauritsen, L.; Olesen, P. H. Scaffold hopping and optimization towards libraries of glycogen synthase kinase-3 inhibitors. *Bioorg. Med. Chem. Lett*. **2002**, *12*, 1525–1528.

(10) Witherington, J., 3-Amino Pyrazoles as Potent and Selective Glycogen Kinase Synthase 3 (GSK-3) Inhibitors. In *Glycogen Synthase Kinase 3* (*GSK-3*) *and Its Inhibitors*; Martinez, A.; Castro, A.; Medina, M., Eds.; John Wiley & Sons, Inc.: New York, 2006; pp 281−305.

(11) Khanfar, M. A.; Abuasal, B.; Mudit, M; Kaddoumi, A; El Sayed, K. Marine natural-derived inhibitors of glycogen synthase kinase-3β phenylmethylene hydantoins: In vitro and in vivo activities, pharmacophore modeling, and virtual screening studies. *Bioorg. Med. Chem*. **2009**, *17*, 6032–6039.

(12) Martinez, A.; Alonso, M.; Castro, A.; Dorronsoro, I.; Gelpi, J. L.; Luque, F. J.; Perez, C.; Moreno, F. J. SAR and 3D-QSAR studies on thiadiazolidinone derivatives: exploration of structural requirements for glycogen synthase kinase 3 inhibitors. *J. Med. Chem*. **2005**, *48*, 7103–7112.

(13) Olesen, P. H.; Sorensen, A. R.; Urso, B.; Kurtzhals, P.; Bowler, A. N.; Ehrbar, U.; Hansen, B. F. Synthesis and in vitro characterization of 1-(4-aminofurazan-3-yl)-5-dialkylaminomethyl-1*H*-[1,2,3]triazole-4-carboxylic acid derivatives. A new class of selective GSK-3 inhibitors. *J. Med. Chem*. **2003**, *46*, 3333–3341.

(14) Berg, S.; Hellberg, S. Preparation of *N*-(4-methoxybenzyl)-*N*′-(5-nitro-1,3-thiazol-2-yl)urea for treating conditions associated with glycogen-synthase kinase-3 (GSK3). PCT Int. Appl. WO 2003004478, 2003.

(15) O'Neill, D. J.; Shen, L.; Prouty, C.; Conway, B. R.; Westover, L.; Xu, J. Z.; Zhang, H. C.; Maryanoff, B. E.; Murray, W. V.; Demarest, K. T.; Kuo, G. H. Design, synthesis, and biological evaluation of novel 7-azaindolyl-heteroaryl-maleimides as potent and selective glycogen synthase kinase-3β (GSK-3β) inhibitors. *Bioorg. Med. Chem*. **2004**, *12*, 3167–3185.

(16) Nuss, J. M.; Harrison, S. D.; Ring, D. B.; Boyce, R. S.; Brown, S. P.; Goff, D.; Johnson, K.; Pfister, K. B.; Ramurthy, S.; Renhowe, P. A.; Seely, L.; Subramanian, S.; Wagman, A. S.; Zhou, X. A. Preparation of aminopyrimidines and -pyridines as glycogen synthase kinase 3 inhibitors. PCT Int. Appl. WO 9965897, 1999.

(17) Gentles, R. G.; Hu, S.; Dubowchik, G. M. Recent advances in the discovery of GSK-3 inhibitors and a perspective on their utility for the treatment of Alzheimer's disease. *Annu. Rep. Med. Chem.* **2009**, *44*, 3–26.
(18) Godemann, R.; Biernat, J.; Mandelkow, E.; Mandelkow, E. M. Phosphorylation of tau protein by recombinant GSK-3beta: pronounced phosphorylation at select Ser/Thr-Pro motifs but no phosphorylation at Ser262 in the repeat domain. *FEBS Lett.* **1999**, *454*, 157–164.
(19) Gong, C. X.; Lidsky, T.; Wegiel, J.; Zuck, L.; Grundke-Iqbal, I.; Iqbal, K. Phosphorylation of microtubule-associated protein tau is regulated by protein phosphatase 2A in mammalian brain. Implications for neurofibrillary degeneration in Alzheimer's disease. *J. Biol. Chem.* **2000**, *275*, 5535–5544.
(20) Iqbal, K.; Grundke-Iqbal, I. Inhibition of neurofibrillary degeneration: A promising approach to Alzheimer's disease and other tauopathies. *Curr. Drug Targets* **2004**, *5*, 495–502.
(21) Phiel, C. J.; Wilson, C. A.; Lee, V.M-Y.; Klein, P. S. GSK-3alpha regulates production of Alzheimer's disease amyloid-beta peptides. *Nature* **2003**, *423*, 435–439.
(22) Takashima, A.; Noguchi, K.; Michel, G.; Mercken, M.; Hoshi, M.; Ishiguro, K.; Imahori, K. Exposure of rat hippocampal neurons to amyloid beta peptide (25−35) induces the inactivation of phosphatidyl inositol-3 kinase and the activation of tau protein kinase I/glycogen synthase kinase-3 beta. *Neurosci. Lett.* **1996**, *203*, 33–36.
(23) Culbert, A, A.; Brown, M. J.; Frame, S.; Hagen, T.; Cross, D. A. E.; Bax, B.; Reith, A. D. GSK-3 inhibition by adenoviral FRAT1 overexpression is neuroprotective and induces tau dephosphorylation and beta-catenin stabilization without elevation of glycogen synthase activity. *FEBS Lett.* **2001**, *507*, 288–294.
(24) Alvarez, G.; Munoz-Montano, J. R.; Satrustegui, J.; Avila, J.; Bogonez, E.; Diaz-Nido, J. Lithium protects cultured neurons against beta-amyloid-induced neurodegeneration. *FEBS Lett.* **1999**, *453*, 260–264.
(25) Medina, M.; Castro, A. Glycogen synthase kinase-3 (GSK-3) 1045 inhibitors reach the clinic. *Curr. Opin. Drug Discovery Dev.* **2008**, *11*, 533–543.
(26) Bertrand, J. A.; Thieffine, S.; Vulpetti, A.; Cristiani, C.; Valsasina, B.; Knapp, S.; Kalisz, H. M.; Flocco, M. Structural characterization of the GSK-3beta active site using selective and non-selective ATP-mimetic inhibitors. *J. Mol. Biol.* **2003**, *333*, 393–407.
(27) Taha, M. O.; Bustanji, Y.; Al-Ghussein, M. A. S.; Mohammad, M.; Zalloum, H.; Al-Masri, I. M.; Atallah, N. Pharmacophore modeling, quantitative structure−activity relationship analysis, and in silico screening reveal potent glycogen synthase kinase-3beta inhibitory activities for cimetidine, hydroxychloroquine, and gemifloxacin. *J. Med. Chem.* **2008**, *51*, 2062–2077.
(28) Kim, H.-J.; Choo, H.; Cho, Y. S.; No, K. T. i.; Pae, A. N. Novel GSK-3beta inhibitors from sequential virtual screening. *Bioorg. Med. Chem.* **2008**, *16*, 636–643.
(29) Patel, D. S.; Bharatam, P. V. New leads for selective GSK-3 inhibition: pharmacophore mapping and virtual screening studies. *J. Comput.-Aided Mol. Des.* **2006**, *20*, 55–66.
(30) Lipinski, C. A.; Lombardo, F.; Dominy, B. W.; Feeney, P. J. Experimental and computational approaches to estimate solubility and permeability in drug discovery and development settings. *Adv. Drug Delivery Rev.* **2001**, *46*, 3–26.
(31) Chekler, E. L. P.; Elokdah, H. M.; Butera, J. Efficient one-pot synthesis of substituted 2-amino-1,3,4-oxadiazoles. *Tetrahedron Lett.* **2008**, *49*, 6709–6711.
(32) van der Waterbeemd, H. Quantitative approaches to structure-activity relationships. In *The Practice of Medicinal Chemistry*; Wermuth, C. G., Ed.; Academic Press: London, 1996; p 367.
(33) Martin, Y. C.; Bures, M. G.; Danaher, E. A.; DeLazzer, J.; Lico, I.; Pavlik, P. A. A fast new approach to pharmacophore mapping and its application to dopaminergic and benzodiazepine agonists. *J. Comput.-Aided Mol. Des.* **1993**, *7*, 83–102.
(34) Clark, R. D. OptiSim: an extended dissimilarity selection method for finding diverse representative subsets. *J. Chem. Inf. Comput. Sci.* **1997**, *37*, 1181–1188.
(35) Marriott, D. P.; Dougall, I. G.; Meghani, P.; Liu, Y.-J.; Flower, D. R. Lead generation using pharmacophore mapping and three-dimensional database searching: application to muscarinic M(3) receptor antagonists. *J. Med. Chem.* **1999**, *42*, 3210–3216.
(36) Spadoni, G.; Balsamini, C.; Diamantini, G.; Di Giacomo, B.; Tarzia, G.; Mor, M.; Plazzi, P. V.; Rivara, S.; Lucini, V.; Nonno, R.; Pannacci, M.; Fraschini, F.; Stankov, B. M. Conformationally restrained melatonin analogues: synthesis, binding affinity for the melatonin receptor, evaluation of the biological activity, and molecular modeling study. *J. Med. Chem.* **1997**, *40*, 1990–2002.
(37) Gadakar, P. K.; Phukan, S.; Dattatreya, P.; Balaji, V. N. Pose prediction accuracy in docking studies and enrichment of actives in the active site of GSK-3beta. *J. Chem. Inf. Model.* **2007**, *47*, 1446–5149.
(38) Polgar, T.; Baki, A.; Szendrei, G. I.; Keseru, G. M. Comparative virtual and experimental high-throughput screening for glycogen synthase kinase-3beta inhibitors. *J. Med. Chem.* **2005**, *48*, 7946–7959.
(39) Bhat, R.; Xue, Y.; Berg, S.; Hellberg, S.; Ormoe, M.; Nilsson, Y.; Radesaeter, A.; Jerning, E.; Markgren, P. O.; Borgegard, T.; Nyloef, M.; Gimenez-Cassina, A.; Hernandez, F.; Lucas, J. J.; Diaz-Nido, J.; Avila, J. Structural insights and biological effects of glycogen synthase kinase 3-specific inhibitor AR-A014418. *J. Biol. Chem.* **2003**, *278*, 45937–45945.
(40) Meijer, L.; Skaltsounis, A. L.; Magiatis, P.; Polychronopoulos, P.; Knockaert, M.; Leost, M.; Ryan, X. P.; Vonica, C. A.; Brivanlou, A.; Dajani, R.; Crovace, C.; Tarricone, C.; Musacchio, A.; Roe, S. M.; Pearl, L.; Greengard, P. GSK-3-Selective inhibitors derived from tyrian purple indirubins. *Chem. Biol.* **2003**, *10*, 1255–1266.
(41) Jain, A. N. Surflex: fully automatic flexible molecular docking using a molecular similarity-based search engine. *J. Med. Chem.* **2003**, *46*, 499–511.
(42) Tripos Associates. *SYBYL Molecular Modeling Software*, version 8.0; Tripos Associates: St. Louis, MO, 2007; http://www.tripos.com.
(43) Jones, G.; Willett, P.; Glen, R. C. Molecular recognition of receptor sites using a genetic algorithm with a description of desolvation. *J. Mol. Biol.* **1995**, *245*, 43–53.
(44) Shultz-Gasch, T.; Stahl, M. Binding site characteristics in structure-based virtual screening: evaluation of current docking tools. *J. Mol. Model.* **2003**, *9*, 47–57.
(45) Rodems, S. M.; Hamman, B. D.; Lin, C.; Zhao, J.; Shah, S.; Heidary, D.; Makings, L.; Stack, J. H.; Pollok, B. A. A FRET-based assay platform for ultra-high density drug screening of protein kinases and phosphatases. *Assay Drug Dev. Technol.* **2002**, *1*, 9–19.
(46) Hamann, M. T.; Alonso, D.; Martín-Aparicio, E.; Fuertes, A.; Pérez-Puerto, J.; Castro, A.; Morales, S.; Navarro, M. L.; del Monte-Millán, M.; Medina, M.; Pennaka, H.; Balaiah, A.; Peng, J.; Cook, J.; Wahyuono, S.; Martínez, A. Glycogen synthase kinase-3 (GSK-3) inhibitory activity and structure−activity relationship (SAR) studies of the manzamine alkaloids. Potential for Alzheimer's disease. *J. Nat. Prod.* **2007**, *70*, 1397–1405.
(47) Lawrie, A. M.; Noble, M. E.; Tunnah, P.; Brown, N. R.; Johnson, L. N.; Endicott, J. A. Protein kinase inhibition by staurosporine revealed in details of the molecular interaction with CDK2. *Nature Struct. Biol.* **1997**, *4*, 796–801.
(48) Ravitz, M. J.; Wenner, C. E. Cyclin-dependent kinase regulation during G1 phase and cell cycle regulation by TGF-beta. *Adv. Cancer Res.* **1997**, *71*, 165–207.
(49) Lochhead, P. A.; Coghlan, M.; Rice, S. Q. J.; Sutherland, C. Inhibition of GSK-3 selectively reduces glucose-6-phosphatase and phosphatase and phosphoenol-ypyruvate carboxykinase gene expression. *Diabetes* **2001**, *50*, 937–946.
(50) Saitoh, M.; Kunitomo, J.; Kimura, E.; Hayase, Y.; Kobayashi, H.; Uchiyama, N.; Kawamoto, T.; Tanaka, T.; Mol, C. D.; Dougan, D. R.; Textor, G. P.; Snell, G. P.; Itoh, F. Design, synthesis and structure−activity relationships of 1,3,4-oxadiazole derivatives as novel inhibitors of glycogen synthase kinase-3β. *Bioorg. Med. Chem.* **2009**, *17*, 2017–2029.
(51) Saitoh, M.; Kunitomo, J.; Kimura, E.; Iwashita, H.; Uno, Y.; Onishi, T.; Uchiyama, N.; Kawamoto, T.; Tanak, T.; Mol, C. D.; Dougan, D. R.; Textor, G. P.; Snell, G. P.; Takizawa, M.; Itoh, F.; Kori, M. 2-{3-[4-(Alkylsulfinyl)phenyl]-1-benzofuran-5-yl}-5-methyl-1,3,4-oxadiazole derivatives as novel inhibitors of glycogen synthase kinase-3β with good brain permeability. *J. Med. Chem.* **2009**, *52*, 6270–6286.
(52) Mylonas, S.; Mamalis, A. Synthesis and antitumor activity of new thiosemicarbazones of 2-acetylimidazo[4,5-*b*]pyridine. *J. Heterocycl. Chem.* **2005**, *42*, 1273–1281.
(53) Carroll, N. V.; Longley, R. W.; Roe, J. H. The determination of glycogen in liver and muscle by use of anthrone reagent. *J. Biol. Chem.* **1956**, *220*, 583–593.